

LEARNING ROBUST CONVOLUTIONAL NEURAL NETWORKS WITH RELEVANT FEATURE FOCUSING VIA EXPLANATIONS

Kazuki Adachi and Shin'ya Yamaguchi

Computer and Data Science Laboratories, NTT Corporation, Japan
{kazuki.adachi, shinya.yamaguchi}@ntt.com

ABSTRACT

Existing image recognition techniques based on convolutional neural networks (CNNs) basically assume that the training and test datasets are sampled from i.i.d distributions. However, this assumption is easily broken in the real world because of the distribution shift that occurs when the co-occurrence relations between objects and backgrounds in input images change. Under this type of distribution shift, CNNs learn to focus on features that are not task-relevant, such as backgrounds from the training data, and degrade their accuracy on the test data. To tackle this problem, we propose *relevant feature focusing (ReFF)*. ReFF detects task-relevant features and regularizes CNNs via explanation outputs (e.g., Grad-CAM). Since ReFF is composed of post-hoc explanation modules, it can be easily applied to off-the-shelf CNNs. Furthermore, ReFF requires no additional inference cost at test time because it is only used for regularization while training. We demonstrate that CNNs trained with ReFF focus on features relevant to the target task and that ReFF improves the test-time accuracy.

Index Terms— Convolutional neural networks, explanations, spurious features

1. INTRODUCTION

Convolutional neural networks (CNNs) have achieved high accuracy in image recognition tasks [1, 2] under the assumption that the training and test datasets are sampled from i.i.d distributions. However, in the real world, this assumption may not be valid and the distributions easily shift because of changing contexts in images such as in the co-occurrences between backgrounds and objects [3, 4, 5]. In such cases, the accuracy of the CNNs is degraded.

One of the causes of distribution shift is using a biased procedure to collect the training dataset. Practitioners often collect training data from biased contexts (e.g., backgrounds) due to budget limitations. A training dataset made within such limitations may have *spurious features*, that are correlated with labels only in the training dataset even though they are originally unrelated to the task [6, 7]. Spurious features can easily vanish or mutate in a test environment where the

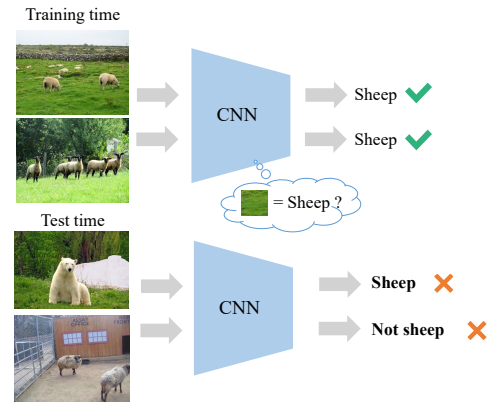


Fig. 1. Example of spurious features. CNNs mistakenly learn the features of grassy fields to be ‘sheep’ because the training images labeled ‘sheep’ tend to contain grassy fields. But at test time, images of non-sheep in grassy fields are classified as ‘sheep’ and vice versa. The images are sampled from the AwA dataset [9].

context changes. If CNNs learn spurious features, their accuracy may be degraded at test time. In such a case, the reliability of the CNNs also deteriorates since they focus on features unrelated to the task. This problem frequently occurs in image recognition because the context may change after the models are deployed [3, 5], as illustrated in Fig. 1. Thus, to train robust and reliable CNNs, it is important to focus on *task-relevant features* that are originally related to the task and are invariant to the training and test distributions [3, 8].

To avoid degradation of accuracy caused by spurious features and improve the reliability at test time, we propose *relevant feature focusing (ReFF)*. ReFF consists of an *explanation regularizer* and a *pseudo-annotator*. The explanation regularizer constrains the CNN classifiers to focus on task-relevant features and avoid spurious features by minimizing the gap between the explanations of the classifiers and regional annotations, which indicate the regions of task-relevant features in the training images. The explanation regularizer can be applied to off-the-shelf CNN classifiers because it uses a post-hoc explanation module for computing the regularization term. Although it can make CNNs focus on task-

relevant features, it requires the regional annotations to be manually created for each training image. Here, we use the pseudo-annotator to reduce the number of regional annotations. The pseudo-annotator detects regions of task-relevant features from the input images and generates regional annotations with an encoder-decoder network inspired by image translation [10]. We experimentally confirmed that a pseudo-annotator trained on only several manual regional annotations can improve the accuracy of the classifiers. We conducted experiments on artificial (Textured MNIST) and real world datasets (ISIC2017 [11], Oxford-IIIT Pets [12]) and confirmed that spurious features affect CNNs especially when the datasets have diverse task-relevant features or the task-relevant features are small in addition to there being a strong correlation between spurious features and labels. Moreover, we found that CNN classifiers trained with ReFF had higher test accuracy in the presence of spurious features by focusing on task-relevant features.

2. RELATED WORK

Domain adaptation: Domain adaptation (DA) [13] is a popular technique for dealing with the distribution shift at test time. It helps models to learn features that are invariant to the source and target datasets. However, DA requires a target dataset collected from the test environment for training. In practice, it is difficult to access the test environment before deploying models. Contrastively, our goal is to train models that generalize to the test environment without accessing it.

Regularizing via attention maps: In the context of explainable AI, several methods to visualize the predictions of CNNs have been developed [14, 15, 16, 17]. These methods have also been used for regularizing CNNs to focus on task-relevant features and to be robust against spurious features [18, 3, 8]. In contrast to DA methods, these regularization methods help CNNs generalize to unseen test datasets without accessing test environments at training time by focusing on task-relevant features. Mitsuhashi et al. [18] used a specialized CNN architecture called ABN [16] for regularizing CNNs via attention maps. They minimized the mean squared errors between attention maps generated by ABN and manual regional annotations. However, since ABN is composed of specialized architectures, it is hard to apply to off-the-shelf architectures. On the other hand, several studies have used post-hoc explanation modules for generating attention maps [3, 8]. Although the post-hoc modules can be adapted to off-the-shelf architectures, these methods require multi-class labels or numerous additional regional annotations (e.g., 30,917 regional annotations in [18]). ReFF uses a post-hoc explanation module and can be applied to single-class labels. Here, with an eye to keeping flexibility, we reduced the number of additional annotations by using a pseudo-annotator built with an image translation model, which is trainable on a smaller number of annotations in Sec. 4.5.

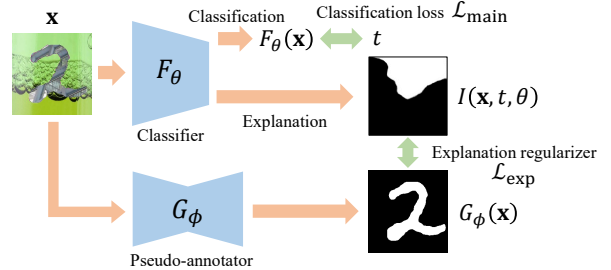


Fig. 2. Overview of relevant feature focusing (ReFF).

3. FOCUSING ON TASK-RELEVANT FEATURE

In this section, we introduce ReFF, which makes CNNs focus on task-relevant features instead of spurious ones. As shown in Fig. 2, ReFF is composed of an *explanation regularizer* and a *pseudo-annotator*. The explanation regularizer minimizes the gap between the explanations of the CNNs and the regional annotations by regularizing multiple intermediate layers in such a way that the CNNs focus on task-relevant features. The pseudo-annotator is an auxiliary model used at training time to detect task-relevant features and generate regional annotations instead of manually collecting them. In practice, a pseudo-annotator can be trained on a reasonable number (hundreds or even dozens) of regional annotations.

3.1. Explanation Regularizer

ReFF regularizes the CNN to focus on task-relevant features via the explanations of the CNN [14, 15, 17]. Explanations were originally designed to interpret the predictions of CNNs. Most explanation methods generate heat maps that indicate regions in the input images that the CNNs focus on. We use these heat maps for regularizing the CNNs. In particular, ReFF uses Grad-CAM [14] as an explanation because it is easy to implement and can be computed from arbitrary intermediate layers of CNNs. We will denote Grad-CAM computed from layer l by $I_l(\mathbf{x}, y, \theta) \in \mathbb{R}_+^{H^l \times W^l}$, where $\mathbf{x} \in \mathbb{R}^{3 \times H \times W}$ is an input image, y is the class label for \mathbf{x} , and θ consists of parameters of the CNN classifier F_θ . $I_l(\mathbf{x}, y, \theta)$ indicates the important region of \mathbf{x} to be classified to y by F_θ . Grad-CAMs are produced by calculating the sum of the feature maps $A^l \in \mathbb{R}^{K^l \times H^l \times W^l}$ weighted by their gradients:

$$I_l(\mathbf{x}, y, \theta) = \text{ReLU} \left(\sum_{k=1}^{K^l} \alpha_k^l A_k^l \right), \quad (1)$$

$$\alpha_k^l = \frac{1}{H^l W^l} \sum_{i,j} \frac{\partial F_\theta(\mathbf{x})_y}{\partial A_{k,i,j}^l}. \quad (2)$$

The explanation regularizer matches $I_l(\mathbf{x}, y, \theta)$ and the regional annotations of \mathbf{x} , denoted by \mathbf{s} , for each layer as follows:

$$\mathcal{L}_{\text{ReFF}} = \mathbb{E}_{\mathbf{x}, y, \mathbf{s}} \left[\sum_{l=1}^L w_l \|I_l(\mathbf{x}, y, \theta) \odot (\mathbf{1} - \mathbf{s})\|_2^2 \right], \quad (3)$$

where \odot is the element-wise product, w_l is a hyperparameter to determine the weight for layer l , and $\mathbf{s} \in [0, 1]^{H \times W}$ is a regional annotation that has the same resolution as \mathbf{x} . \mathbf{s} is 1 for regions of task-relevant features and 0 for other regions. $I'_l(\mathbf{x}, y, \theta)_{i,j} = I_l(\mathbf{x}, y, \theta)_{i,j} / \|I_l(\mathbf{x}, y, \theta)\|_1$ is the normalized explanation. Since each $I_l(\mathbf{x}, y, \theta)$ has a different resolution, we resize it to the same resolution as \mathbf{s} by linear interpolation. While previous studies [8, 18] strictly match explanations and regional annotations simply by minimizing their L1 or L2 error, we minimize the norm of the explanations only outside the regions of the task-relevant features to enable the CNNs to implicitly learn the importance of the task-relevant features inside the regions. In fact, we found that aligning $I(\mathbf{x}, y, \theta)$ and \mathbf{s} by using the L1 or L2 error instead of $\mathcal{L}_{\text{ReFF}}$ has a negative effect (see Sec. B of the supplementary materials) because each pixel inside the regions of the task-relevant features has a different importance, while \mathbf{s} usually contains binary values that does not represent the importance. In addition, we designed the explanation regularizer to penalize multiple layers of CNNs because each layer extracts the features of different levels, from low-level textures to high-level discriminative objects [19, 20]. By regularizing the explanations of multiple layers simultaneously, F_θ can learn various levels of task-relevant feature. We add $\mathcal{L}_{\text{ReFF}}$ to main objective $\mathcal{L}_{\text{main}}$, the whole objective is $\mathcal{L} = \mathcal{L}_{\text{main}} + \lambda \mathcal{L}_{\text{ReFF}}$, where λ is a hyperparameter to balance the main loss term and the regularization term.

3.2. Pseudo-annotator

The explanation regularizer in Eq. (3) requires a regional annotation \mathbf{s} for each image. To reduce the number of regional annotations, we incorporate a pseudo-annotator $G_\phi : \mathbb{R}^{3 \times H \times W} \mapsto [0, 1]^{H \times W}$, which generates pseudo-annotations of \mathbf{s} for the explanation regularizer. We regard this pseudo-annotation generation task as an image-translation that maps an input image to a pseudo-annotation. We use pix2pix [10] for the image-translation. Pix2pix is a supervised image-translation method. The experimental results reported in [10] show that pix2pix can be trained on a small dataset consisting of hundreds of images. We expect that the pseudo-annotator can be trained with the same order of images. After training G_ϕ , a pseudo-annotation $G_\phi(\mathbf{x})$ is used for samples that do not have \mathbf{s} as Eq. (4) instead of Eq. (3).

$$\mathcal{L}_{\text{ReFF}} = \mathbb{E}_{\mathbf{x}, y} \left[\sum_{l=1}^L w_l \|I'_l(\mathbf{x}, y, \theta) \odot (\mathbf{1} - G_\phi(\mathbf{x}))\|_2^2 \right]. \quad (4)$$

4. EXPERIMENTS

We identify when spurious features affect CNNs and confirm that ReFF helps CNNs to learn task-relevant features and avoid the effect of spurious features. First, we examine the effect of the explanation regularizer on Textured MNIST

directly by using regional annotations without the pseudo-annotator. Then, we test the pseudo-annotator on all datasets to evaluate the total effect of ReFF.

4.1. Datasets

We used three datasets: Textured MNIST, ISIC2017 [11], and Oxford-IIIT Pet (Pets) [12]. Textured MNIST is an artificial dataset we made, the others are real-world datasets.

Textured MNIST is composed of MNIST [21] and DTD [22] for the purpose of assessing the effect of spurious features by controlling co-occurrences of digits and background textures. We placed a digit image from MNIST in a 224×224 canvas and put different texture images from DTD on each of the digit and the background. The task is to classify the images into 10 digit classes without being affected by background textures. We simulated spurious features by fixing the classes of background textures corresponding to each digit class. Thus, backgrounds are spurious features correlated with the digit classes. We controlled the degree of effect of the spurious features with a background texture randomness p and a digit texture randomness q . We selected a background texture from a random class with probability p and selected another background texture from the fixed class corresponding to the digit class with probability $1 - p$. We also selected the textures of the digits in the same way with probability q . When p is small, the images in the dataset have strong spurious features that CNNs will likely learn even though they are originally not related to digit classification. A larger q generates a wider diversity of task-relevant features and makes the spurious features more discriminative than the task-relevant ones. In the test dataset, p is set to 1 so that the correlation between the spurious features and the labels is broken. Further, we controlled the size of the digits to evaluate the effect of the size of the task-relevant features.

ISIC2017 [11] is a dataset consisting of three classes of skin lesion image. Some of the images contain not only lesions but also artifacts such as colorful patches, scales, and markers [23]. These artifacts can be regarded as spurious features.

Oxford-IIIT Pet (Pets) [12] is a dataset consisting of images of cats and dogs, classified into 37 classes. We selected this dataset as an example of a natural dataset that does not have trivial spurious features, unlike ISIC2017.

Sec. A of the supplementary materials provides details on and examples from the datasets.

4.2. Training Details

Classification: We used ResNet-50 [24] pretrained on ImageNet [25] for the classifier. We applied the explanation regularizer to the outputs of the blocks of `layer1` to `layer4`. We set the weights for each layer in Eq. (3) $\lambda = 1$ and $(w_1, w_2, w_3, w_4) = (15, 60, 250, 1000)$, where λ was set as such to make $\mathcal{L}_{\text{ReFF}}$ and $\mathcal{L}_{\text{main}}$ roughly of the same order and w_i is for balancing the importance of the layers. For w_i , we

Table 1. Test accuracy [%] on Textured MNIST. For each condition, we ran the training three times with different random seeds, the standard deviations are shown together.

(a) vs background randomness $p(q=1)$			(b) vs digit texture randomness $q(p=0)$		
p	Baseline	ReFF	q	Baseline	ReFF
0.0	31.29±2.16	46.68±0.82	0.0	45.39±0.63	62.34±2.65
0.2	99.44±0.06	99.47±0.06	0.2	36.18±0.54	51.80±3.99
0.4	99.51±0.05	99.33±0.10	0.4	32.02±1.22	49.25±0.57
0.6	99.50±0.02	99.60±0.04	0.6	31.53±1.72	47.10±2.04
0.8	99.46±0.02	99.55±0.02	0.8	32.79±4.66	49.92±4.22
1.0	99.53±0.03	99.46±0.08	1.0	30.80±1.33	46.44±1.01

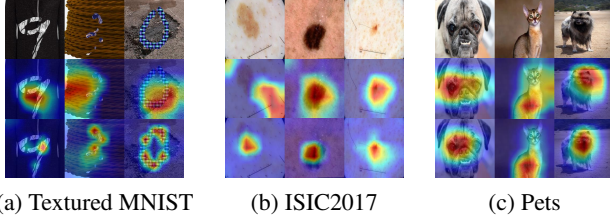


Fig. 3. Grad-CAMs computed from the outputs of `layer4`. The red regions indicate where the classifiers attach importance in order to make a prediction, the blue regions are the opposite. The upper, middle, and lower rows show the inputs, baseline, and ReFF, respectively.

found that assigning larger weights to higher layers produced better results by performing a grid search. For the objective, we implemented $\mathcal{L}_{\text{main}}$ with cross entropy.

Pseudo-annotator: We used U-Net [26] for the pseudo-annotator G_ϕ in the same way as [10].

The detailed settings are in Sec. D of the supplementary materials.

4.3. Effect of Spurious Features

We evaluate the accuracy of the CNNs under various degrees of spurious features. We trained the classifiers on Textured MNIST by varying the background randomness p and the digit texture randomness q in the training dataset. We fixed the digit size to 223. We compared ReFF with a baseline that minimizes only the cross entropy loss. First, we fixed $q = 1$ and varied p to evaluate the effect of spurious features. Tab. 1 (a) shows the test accuracies with respect to p . When $p > 0$ in the training dataset, both the baseline and ReFF achieve high accuracy. However, when $p = 0$ (fixed background textures), the accuracy drops because the correlation between the spurious features and labels is strong in the training dataset. Here, ReFF alleviated the accuracy drop by preventing the classifiers from learning the spurious features. Next, we set $p = 0$ and varied the digit texture randomness q to evaluate the effect of the variety of task-relevant features under strong spurious features. In this setting, when q is higher, the test is more difficult because the spurious features (fixed textures of backgrounds) are more discriminative

Table 2. Test accuracy [%] vs. digit size on Textured MNIST.

Digit size	Baseline	ReFF	ReFF
		(single layer)	(multi-layers)
28	10.25±0.51	10.19±0.31	10.32±0.23
56	12.02±0.57	12.15±1.03	13.86±1.37
112	18.66±0.34	21.22±1.56	22.64±0.70
168	25.81±0.97	32.67±1.63	36.58±3.06
223	28.45±1.66	40.98±1.66	45.99±1.55

than the task-relevant features (randomly sampled textures of digits). Tab. 1 (b) shows the results. Here, the baseline model learned spurious features and the test accuracy deteriorated as q increased. On the other hand, ReFF achieved a higher test accuracy than the baseline model by about 15%pt in all cases. This suggests that ReFF can learn task-relevant features even when strong spurious features exist in the training dataset. The effect of ReFF can also be seen in the explanations of the models. Fig. 3 (a) shows the Grad-CAMs of the test data generated from the classifier trained on $p = 0$. As shown in the middle row, the baseline model focused on background textures that are unrelated to digit classification. This is because the background textures are discriminative features only in the training dataset. In contrast, as shown in the bottom row, the CNN trained with ReFF properly focused on digits. We also evaluate ReFF with additional cases (Sec. C of the supplementary materials).

4.4. Effect of the Size of the Task-Relevant Features

We varied the size of the digits of Textured MNIST to show that applying ReFF regularization to multiple layers simultaneously enables various sizes of task-relevant feature to be learned. We set $(p, q) = (0, 1)$ for the training dataset and $(p, q) = (1, 1)$ for the test dataset, where the effect of spurious features is the strongest. We placed the digits at random positions in each image. Tab. 2 shows the test accuracies. We compared ReFF with its variant, which uses only `layer4` in Eq. (3) with $\lambda = 1000$ and $w_{\text{layer4}} = 1$. When the digit size ≥ 112 , ReFF with multi-layers and ReFF with a single layer improved the test accuracy. But ReFF with multi-layers was the more accurate. Especially for a digit size of 56, it showed an accuracy improvement over the baseline while the accuracy of ReFF with a single layer stayed almost the same as that of the baseline. This means that regularizing lower layers can capture finer task-relevant features better than regularizing only a higher layer. Since the resolution of the feature maps of higher layers become coarser by the stride of the convolutions, capturing fine task-relevant features with only a single high layer is difficult. On the other hand, for a digit size of 28, the accuracies of the baseline and ReFF are both deteriorated and their difference was smaller. This means that ReFF works effectively when the regions of task-relevant features are large. When the task-relevant features are small and buried in spurious features (backgrounds) like in this case, the

Table 3. Test accuracy [%] vs. training subset size n in the case of using the pseudo-annotator.

(a) Comparison of baseline and ReFF on three datasets.

The best accuracy of all and the best accuracy of ReFF are respectively in **bold** and underlined.

n	Textured MNIST	ISIC2017	Pets
0	30.80±1.33	73.00±2.09	92.07±0.35
1	50.25±2.65	75.50±0.33	91.86±0.44
5	52.09±4.96	75.22±1.90	<u>92.00±0.41</u>
10	56.73±8.10	74.78±1.06	91.63±0.22
20	53.88±1.41	76.11±0.79	91.77±0.37
50	51.81±1.10	76.06±1.68	91.83±0.23
All	46.44±1.01	75.61±0.19	91.61±0.45

(b) Comparison of ReFF and ABN-based regularization [18].

n	ReFF	ABN
0	30.80±1.33	33.8±2.57
1	50.25±2.65	43.88±2.19
5	52.09±4.96	41.40±2.54
10	56.73±8.10	43.42±2.44
20	53.88±1.41	44.25±3.97
50	51.81±1.10	45.44±4.59
All	46.44±1.01	53.23±4.77

accuracy of ReFF gets closer to that of the baseline. Note that this is an artificial extreme case that hardly occurs in natural datasets, as evidenced by the experiments on ISIC2017 and Pets described below.

4.5. Effect of Adding the Pseudo-annotator

We evaluate the effect of incorporating the pseudo-annotator G_ϕ in terms of the number of regional annotations. First, we trained G_ϕ on subsets of the training dataset with regional annotations s . We varied the size of the subsets of the training dataset, which means the number of manually collected regional annotations. We made the subsets by sampling $n \in \{0, 1, 5, 10, 20, 50, \text{All}\}$ images *per class* from the training dataset. Then, we trained the CNN classifiers with the trained G_ϕ . In this step, we used all of the training data, but gave regional annotations s for only the subset selected in the former step. For the samples with s , we calculated the explanation regularizer term as Eq. (3). For the rest, we used $G_\phi(\mathbf{x})$ instead of s as Eq. (4). The detailed training procedure is described in Alg. 1 in the supplementary materials. Note that $n = 0$ means that no regional annotations are used (i.e., baseline), and $n = \text{‘All’}$ means that ReFF uses regional annotations directly for all training data without the pseudo-annotator. For Textured MNIST, we set $(p, q) = (0, 1)$ for the training dataset, where the effect of spurious features is the strongest. For the test dataset, we set $(p, q) = (1, 1)$, where spurious features do not exist. Tab. 3 (a) shows the test accuracy on the three datasets trained with and without the pseudo-annotator. For Textured MNIST, ReFF significantly improved the test accuracy in comparison with the baseline ($n = 0$) in spite of the strong spurious features in the training dataset. Even when $n = 1$, where the pseudo-annotator was trained on only 10 ($= 1$ sample per class $\times 10$ class) samples,

ReFF exceeded the baseline by about 20%pt. More interestingly, the $1 \leq n \leq 50$ cases outperformed the $n = \text{‘All’}$ case, which uses regional ones directly. For this reason, we consider that pseudo-annotations are more informative than regional annotations. While regional annotations have binary values indicating the regions of task-relevant features, the pseudo-annotator outputs ‘soft’ pseudo-annotations that represent the importance of each pixel. For ISIC2017, ReFF also improved accuracy compared with the baseline even when $n = 1$, where the pseudo-annotator was trained on only 3 samples. We can also find cases in which it outperforms the $n = \text{‘All’}$ case. As shown by the Grad-CAMs in Fig. 3 (b), the ReFF model focused on lesions correctly while the baseline model highlighted areas outside the lesions. For Pets, ReFF achieved competitive accuracy with the baseline especially when $n = 5$. This is because we fine-tuned the ImageNet-pretrained model. Since ImageNet contains images of dogs and cats, the ImageNet-pretrained model has already learned task-relevant features as well as ReFF with this dataset. On the other hand, ReFF improved explainability, as shown in Fig. 3 (c). The baseline model sometimes focused on backgrounds, which were originally independent of the classification, whereas the ReFF model highlighted animals more accurately. Thus, the ReFF model generated clear and explanations, which improves reliability.

We also compared ReFF with the ABN-based regularization method [18] (denoted by ABN) on Textured MNIST. Tab. 3 (b) shows the result. ABN uses only manual regional annotations, so we also combined it with our pseudo-annotator. When $n = \text{‘All’}$, where regional annotations are given for all training data, ABN exceeded ReFF because ABN learned accurate attentions with its specialized module called attention branch that is independent of the predictions. On the other hand, when $n \leq 50$ where pseudo-annotations are sometimes inaccurate, ReFF outperformed ABN. This is because our explanation regularizer is robust to corruption of the pseudo-annotations because it suppresses explanations only outside the regions of task-relevant features, as mentioned in Sec. 3.1. Contrastively, since ABN minimizes the L2 error between regional annotations and attentions, the model attempts to align its attentions with the corrupted pseudo-annotations strictly and fails to focus on task-relevant features. We also compared variants of ReFF and visualized the pseudo-annotations, Grad-CAMs, and attentions of ABN (see Sec. B of the supplementary materials).

5. CONCLUSION

We developed ReFF for training CNN classifiers that are robust to changes in spurious features. ReFF regulates the explanations of the classifiers to learn task-relevant features. In addition, it detects task-relevant features and generates pseudo-annotations with a pseudo-annotator trained on a

small number of regional annotations. We experimentally showed that ReFF efficiently learns task-relevant features from training datasets even when strong spurious features exist. ReFF made accurate predictions on the test datasets and improved explanations even when the spurious features vanished or mutated. Moreover, we found that pseudo-annotations further improved the test accuracy beyond that of using regional annotations. In the future, we will explore the effect of the pseudo-annotator and improve ReFF to allow models to learn task-relevant features more efficiently.

6. REFERENCES

- [1] Yann LeCun, Léon Bottou, Yoshua Bengio, and Patrick Haffner, "Gradient-based learning applied to document recognition," *Proceedings of the IEEE*, vol. 86, no. 11, pp. 2278–2324, 1998.
- [2] Alex Krizhevsky, Ilya Sutskever, and Geoffrey E Hinton, "Imagenet classification with deep convolutional neural networks," in *Advances in Neural Information Processing Systems*, 2012.
- [3] Krishna Kumar Singh, Dhruv Mahajan, Kristen Grauman, Yong Jae Lee, Matt Feiszli, and Deepti Ghadiyaram, "Don't Judge an Object by Its Context: Learning to Overcome Contextual Bias," in *the Conference on Computer Vision and Pattern Recognition*, 2020.
- [4] Jinwoo Choi, Chen Gao, Joseph C. E. Messou, and Jia-Bin Huang, "Why Can't I Dance in the Mall? Learning to Mitigate Scene Bias in Action Recognition," in *Advances in Neural Information Processing Systems*, 2019.
- [5] Hyojin Bahng, Sanghyuk Chun, Sangdoon Yun, Jaegul Choo, and Seong Joon Oh, "Learning de-biased representations with biased representations," in *International Conference on Machine Learning*, 2020.
- [6] Yining Chen, Colin Wei, Ananya Kumar, and Tengyu Ma, "Self-training Avoids Using Spurious Features Under Domain Shift," in *Advances in Neural Information Processing Systems*, 2020.
- [7] Chunting Zhou, Xuezhe Ma, Paul Michel, and Graham Neubig, "Examining and Combating Spurious Features under Distribution Shift," in *International Conference on Machine Learning*, 2021.
- [8] Laura Rieger, Chandan Singh, W James Murdoch, and Bin Yu, "Interpretations are useful: penalizing explanations to align neural networks with prior knowledge," in *International Conference on Machine Learning*, 2020.
- [9] Yongqin Xian, Christoph H Lampert, Bernt Schiele, and Zeynep Akata, "Zero-shot learning—A comprehensive evaluation of the good, the bad and the ugly," *IEEE transactions on pattern analysis and machine intelligence*, vol. 41, no. 9, pp. 2251–2265, 2018.
- [10] Phillip Isola, Jun-Yan Zhu, Tinghui Zhou, and Alexei A. Efros, "Image-To-Image Translation With Conditional Adversarial Networks," in *the Conference on Computer Vision and Pattern Recognition*, 2017.
- [11] Noel CF Codella, David Gutman, M Emre Celebi, Brian Helba, Michael A Marchetti, Stephen W Dusza, Aadi Kalloo, Konstantinos Liopyris, Nabin Mishra, Harald Kittler, et al., "Skin lesion analysis toward melanoma detection: A challenge at the 2017 international symposium on biomedical imaging (isbi), hosted by the international skin imaging collaboration (isic)," in *International Symposium on Biomedical Imaging (ISBI)*, 2018.
- [12] Omkar M. Parkhi, Andrea Vedaldi, Andrew Zisserman, and C. V. Jawahar, "Cats and dogs," in *the Conference on Computer Vision and Pattern Recognition*, 2012.
- [13] Gabriela Csurka, "Domain adaptation for visual applications: A comprehensive survey," *arXiv preprint arXiv:1702.05374*, 2017.
- [14] Ramprasaath R. Selvaraju, Michael Cogswell, Abhishek Das, Ramakrishna Vedantam, Devi Parikh, and Dhruv Batra, "Grad-CAM: Visual Explanations From Deep Networks via Gradient-Based Localization," in *International Conference on Computer Vision*, 2017.
- [15] Bolei Zhou, Aditya Khosla, Agata Lapedriza, Aude Oliva, and Antonio Torralba, "Learning Deep Features for Discriminative Localization," in *the Conference on Computer Vision and Pattern Recognition*, 2016.
- [16] Hiroshi Fukui, Tsubasa Hirakawa, Takayoshi Yamashita, and Hironobu Fujiyoshi, "Attention Branch Network: Learning of Attention Mechanism for Visual Explanation," in *the Conference on Computer Vision and Pattern Recognition*, 2019.
- [17] Mukund Sundararajan, Ankur Taly, and Qiqi Yan, "Axiomatic attribution for deep networks," in *International Conference on Machine Learning*, 2017.
- [18] Masahiro Mitsuhara, Hiroshi Fukui, Yusuke Sakashita, Takanori Ogata, Tsubasa Hirakawa, Takayoshi Yamasita, and Hironobu Fujiyoshi, "Embedding Human Knowledge into Deep Neural Network via Attention Map," in *International Conference on Computer Vision Theory and Applications*, 2021.
- [19] Matthew D Zeiler and Rob Fergus, "Visualizing and understanding convolutional networks," in *European conference on computer vision*, 2014.
- [20] Jason Yosinski, Jeff Clune, Yoshua Bengio, and Hod Lipson, "How transferable are features in deep neural networks?," in *Advances in Neural Information Processing Systems*, 2014.
- [21] Yann LeCun, Corinna Cortes, and Christopher J.C. Burges, "MNIST handwritten digit database," 1998, <http://yann.lecun.com/exdb/mnist/>.
- [22] M. Cimpoi, S. Maji, I. Kokkinos, S. Mohamed, , and A. Vedaldi, "Describing Textures in the Wild," in *the Conference on Computer Vision and Pattern Recognition*, 2014.
- [23] Amirreza Mahbod, Gerald Schaefer, Chunliang Wang, Rupert Ecker, and Isabella Ellinge, "Skin lesion classification using hybrid deep neural networks," in *International Conference on Acoustics, Speech and Signal Processing*, 2019.
- [24] Kaiming He, Xiangyu Zhang, Shaoqing Ren, and Jian Sun, "Deep residual learning for image recognition," in *the Conference on Computer Vision and Pattern Recognition*, 2016.
- [25] Olga Russakovsky, Jia Deng, Hao Su, Jonathan Krause, Sanjeev Satheesh, Sean Ma, Zhiheng Huang, Andrej Karpathy, Aditya Khosla, Michael Bernstein, Alexander C. Berg, and Li Fei-Fei, "ImageNet Large Scale Visual Recognition Challenge," *International Journal of Computer Vision*, vol. 115, no. 3, pp. 211–252, 2015.
- [26] Olaf Ronneberger, Philipp Fischer, and Thomas Brox, "U-net: Convolutional networks for biomedical image segmentation," in *International Conference on Medical image computing and computer-assisted intervention*, 2015.

SUPPLEMENTARY MATERIALS FOR LEARNING ROBUST CONVOLUTIONAL NEURAL NETWORKS WITH RELEVANT FEATURE FOCUSING VIA EXPLANATIONS

Kazuki Adachi and Shin'ya Yamaguchi

Computer and Data Science Laboratories, NTT Corporation, Japan
{kazuki.adachi, shinya.yamaguchi}@ntt.com

This manuscript is the supplementary materials of “Learning Robust Convolutional Neural Networks with Relevant Feature Focusing via Explanations”. Sec. A provides the details on the datasets used in the experiments of the main paper. Sec. B provides the additional experiments with variants of ReFF. Sec. C provides the additional experiments on Textured MNIST. Sec. D provides the details of the models used in the experiment and step-by-step procedure of the training.

A. DATASETS

Table 1. Details of the texture classes and the correspondence between the texture classes of DTD and digit classes of MNIST.

Digit	Texture	Background textures
0	banded	blotchy, braided, bubbly, bumpy,
1	dotted	chequered, cobwebbed, cracked,
2	grid	crosshatched, crystalline, fibrous,
3	knitted	flecked, freckled, frilly, gauzy,
4	paisley	grooved, honeycombed, interlaced,
5	scaly	lacelike, lined, marbled, matted,
6	striped	meshed, perforated, pitted, plated,
7	veined	polka-dotted, porous, potholed.
8	woven	smearred, spiralled, sprinkled,
9	zigzagged	stained, stratified, studded,
		swirly, waffled, wrinkled

Textured MNIST has 60,000 images for training and 10,000 images for testing, similar to MNIST. We split the training set into 90% for training and 10% for validation. From DTD, we selected 10 classes for digit texture and the remaining 37 classes for background texture. The shapes of the digits were used as the regional annotations. The names of the texture classes and the correspondence between the digit classes and texture classes are shown in Tab. 1

ISIC2017 contains 2,000 images for training, 150 images for validation, and 600 images for testing. In addition to the class labels, the images also have segmentations that indicate the regions of the lesions, which we regarded as regional annotations.

tions.

Oxford-IIIT Pet (Pets) contains 3,680 images for training and 3,669 images for testing. We randomly split the training set into 90% for training and 10% for validation. Also, each pixel of each image in this dataset is classified into background, foreground, and indeterminate. We made the regional annotations by regarding foreground pixels as task-relevant features and the other pixels as not relevant.

Fig. 1 shows examples of the datasets and corresponding regional annotations explained in Sec. 4.1.

B. EXPLANATION REGULARIZER

To show the effectiveness of our explanation regularizer, we compared with its variants. We replaced the explanation regularizer $\mathcal{L}_{\text{ReFF}}$ described in Sec. 3.1 with the simple L1 or L2 error as follows:

$$\begin{aligned} \mathcal{L}_{L1} &= \mathbb{E}_{\mathbf{x}, y, \mathbf{s}} \left[\sum_{l=1}^L w_l \|I'_l(\mathbf{x}, y, \theta) - \mathbf{s}\|_1 \right], \\ \mathcal{L}_{L2} &= \mathbb{E}_{\mathbf{x}, y, \mathbf{s}} \left[\sum_{l=1}^L w_l \|I'_l(\mathbf{x}, y, \theta) - \mathbf{s}\|_2^2 \right]. \end{aligned}$$

\mathcal{L}_{L1} and \mathcal{L}_{L2} directly minimize the norm of the differences between a regional annotation and a Grad-CAM, whereas $\mathcal{L}_{\text{ReFF}}$ in Eq. (3) minimizes the norm of masked Grad-CAM itself. We set the coefficient $\lambda = 10^{-6}$ for \mathcal{L}_{L1} and \mathcal{L}_{L2} , which produced the best accuracy within $\lambda \in \{10^{-8}, 10^{-7}, 10^{-6}, 10^{-5}\}$. We set $(w_1, w_2, w_3, w_4) = (15, 60, 250, 1000)$, as described in Sec. 4.2.

We also compared ReFF with ABN-based regularization (ABN) [3, 4]. While ABN uses only manual regional annotations, we combined it with our pseudo-annotator. ABN minimizes the L2 error between the attention map $M(\mathbf{x})$ and the regional annotation \mathbf{s} :

$$L_{\text{map}} = \gamma \|M(\mathbf{x}) - \mathbf{s}\|_2^2.$$

Note that L_{map} regularizes only the attention maps generated from a single attention branch module, while \mathcal{L}_{L1} and \mathcal{L}_{L2} regularize the Grad-CAMs generated from multiple layers. For

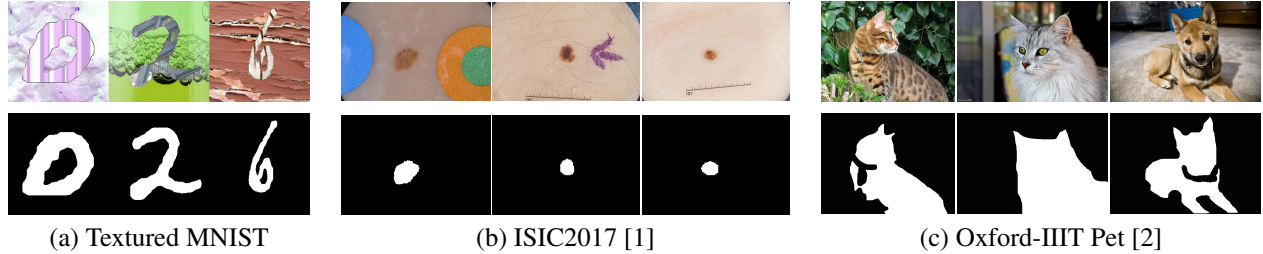


Fig. 1. Examples of the datasets. The upper and lower rows show the images and the corresponding regional annotations for task-relevant features.

Table 2. Test accuracy [%] vs size of training set for pseudo-annotator n on Textured MNIST. The best accuracy for each n is in **boldface**.

n	ReFF	ReFF (L1)	ReFF (L2)	ABN [3]
1	50.25 \pm 2.65	50.43 \pm 1.19	45.21 \pm 2.45	43.88 \pm 2.19
5	52.09 \pm 4.96	51.47 \pm 0.82	44.80 \pm 2.53	41.40 \pm 2.54
10	56.73 \pm 8.10	53.39 \pm 3.17	45.42 \pm 2.10	43.42 \pm 2.44
20	53.88 \pm 1.41	55.01 \pm 1.55	47.78 \pm 0.28	44.25 \pm 3.97
50	51.81 \pm 1.10	46.27 \pm 1.38	47.51 \pm 0.57	45.44 \pm 4.59
All	46.44 \pm 1.01	43.22 \pm 1.08	42.49 \pm 0.98	53.23 \pm 4.77

training, L_{map} was added to the classification loss. We set the hyperparameter $\gamma = 10$, which produced the best accuracy within $\gamma \in \{1, 10, 100\}$. We used ResNet-50 as the backbone of ABN.

We trained the models with these methods on TexturedMNIST in the same way as described in Sec. 4.6. We set the background randomness and digit texture randomness $(p, q) = (0, 1)$ for the training and $(p, q) = (1, 1)$ for the test. We also added a pseudo-annotator trained on the subsets of the training dataset.

Tab. 2 shows the test accuracy. When $n \leq 50$ where the pseudo-annotations are sometimes inaccurate, ReFF achieves the highest accuracy in most cases. This is because ReFF in Eq. (3) is robust to corruption of the pseudo-annotations since it suppresses explanations only outside the regions of task-relevant features as mentioned in Sec 3.1. In the case of the L1 or L2 error, the models attempt to align their attentions with the corrupted pseudo-annotations strictly and fail to focus on task-relevant features. On the other hand, when $n = \text{'All'}$ where regional annotations are given for all training data, ABN outperformed ReFF because ABN has the specialized module called attention branch that is independent of prediction. ReFF (L1) and ReFF (L2) almost degrade the accuracy in comparison with ReFF because regularizing Grad-CAMs with L1 or L2 error has serious effect on accuracy since the feature maps are shared to output Grad-CAMs and the predictions, unlike ABN.

Fig. 2 – Fig. 6 visualize the pseudo-annotations, Grad-CAMs, and attentions of the trained models. As n becomes smaller, while the pseudo-annotations become less accurate as shown in Fig. 2, the Grad-CAMs of ReFF in Fig. 3 high-

light the digits. On the other hand, the attentions of ABN in Fig. 6 highlight the digits accurately when n is large. But the attentions are corrupted when $n = 1$ in contrast to ReFF. Regarding ReFF (L1) and ReFF (L2), the Grad-CAMs in Fig. 4 and Fig. 5 highlight mostly only the central area regardless of n because the models fail to cope with the prediction and focusing on task-relevant features at the same time, since the feature maps are shared to generate the Grad-CAMs and the predictions.

Further, to check whether a model trained with ReFF actually learns the relevant features, not just memorizes the positions of the digits, we also visualize Grad-CAMs for the model trained on Textured MNIST whose digit size is 112. Fig. 7 shows the Grad-CAMs. We can see that the Grad-CAMs highlight the digits regardless of their positions. Hence, we can say that the model trained with ReFF learns the relevant features.

C. EFFECT OF TASK-RELEVANT FEATURES

We evaluated the effect of ReFF under the condition that spurious features does not exist and the task-relevant features vary. Here, we conducted the experiment on Textured MNIST. We fixed background randomness $p = 0$ and varied the digit texture randomness q in Textured MNIST. For the training dataset, we fixed the background randomness $p = 1$ and varied the digit texture randomness q . For the test dataset, we fixed $p = 1$ and set the same q as that of the training dataset. Tab. 3 shows the test accuracies without spurious features in the training dataset ($p = 1$). The baseline and ReFF achieved almost same accuracy ($> 99\%$). This result means

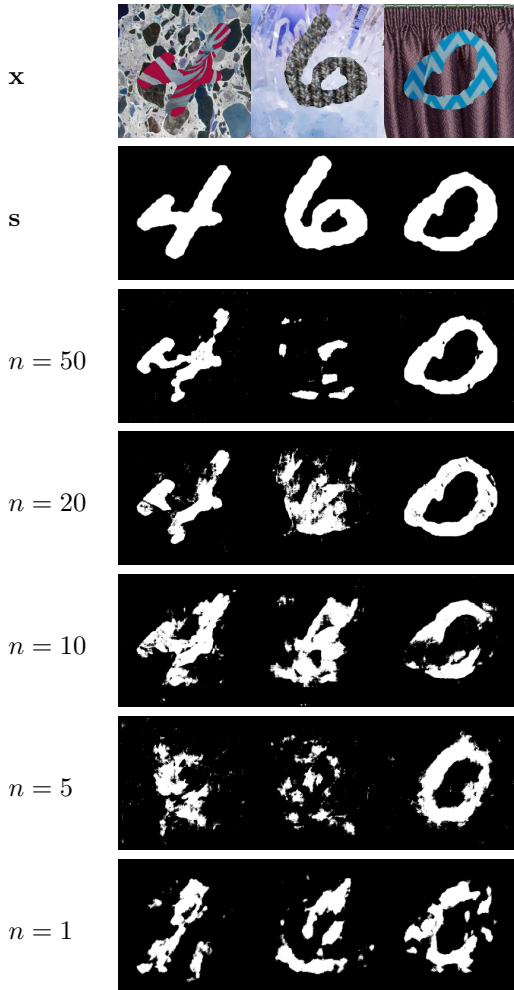


Fig. 2. Examples of pseudo-annotations.

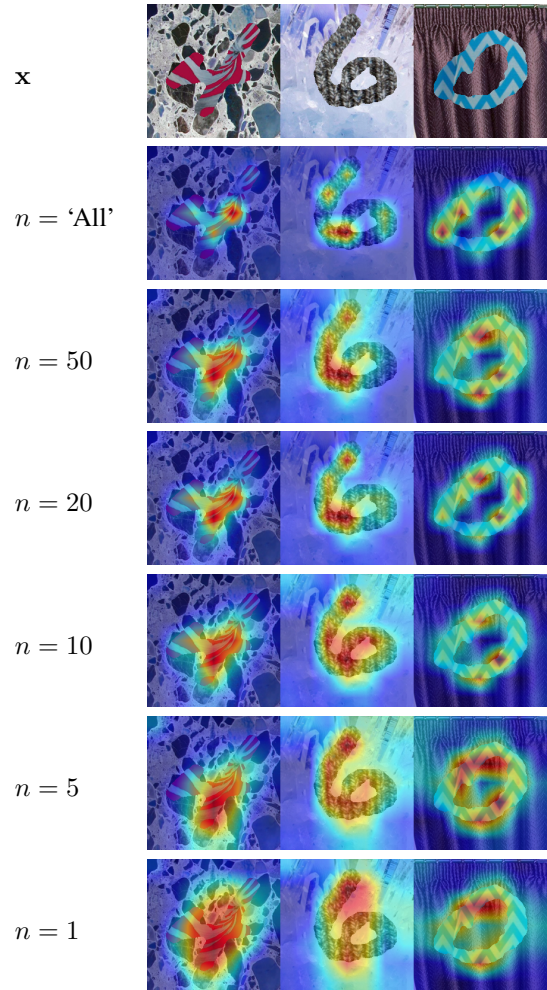


Fig. 3. Grad-CAM examples of ReFF.

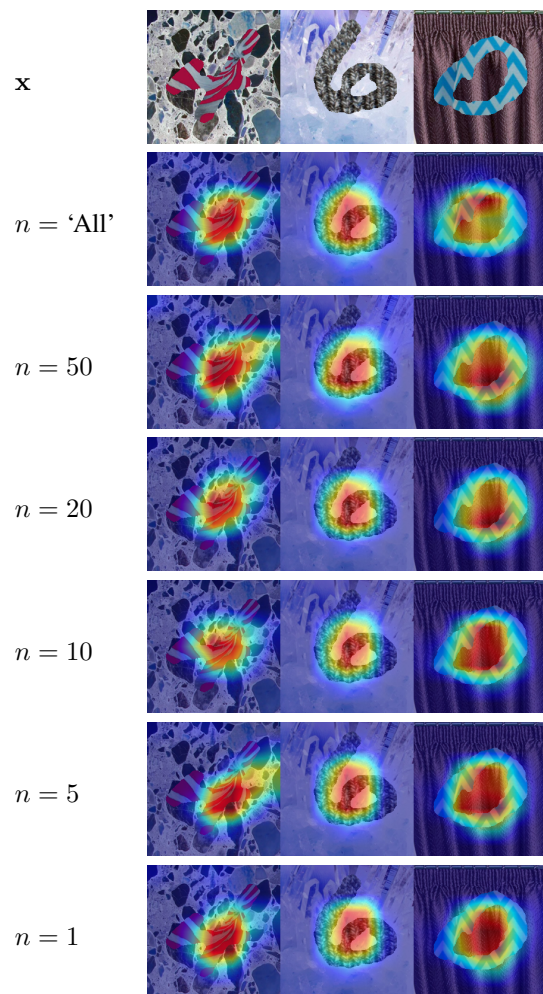


Fig. 4. Grad-CAM examples of ReFF (L1).

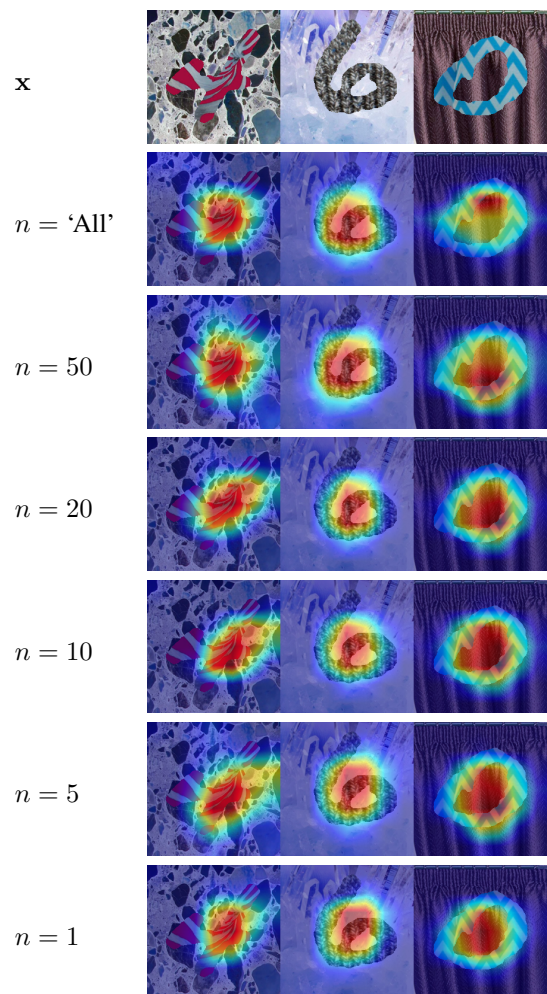


Fig. 5. Grad-CAM examples of ReFF (L2).

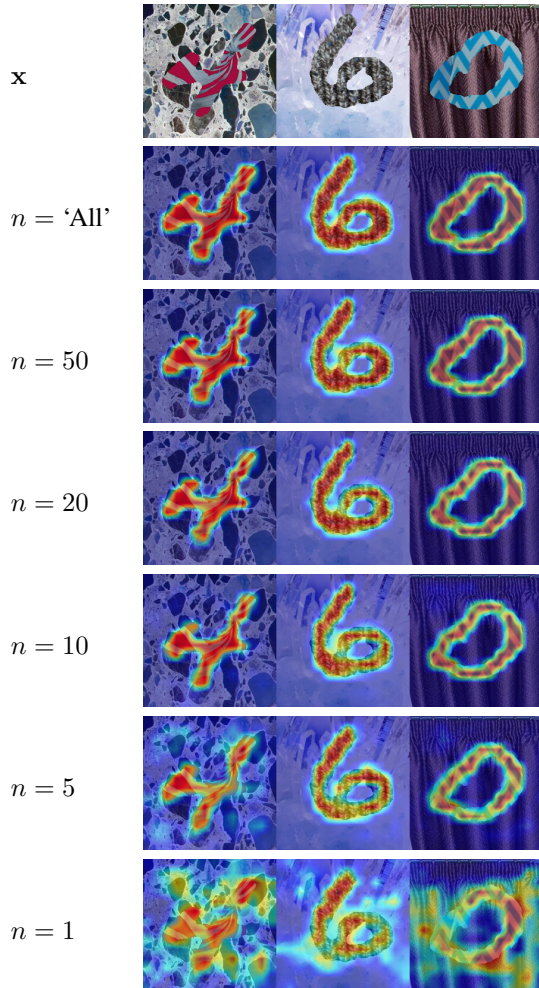


Fig. 6. Attention examples of ABN.

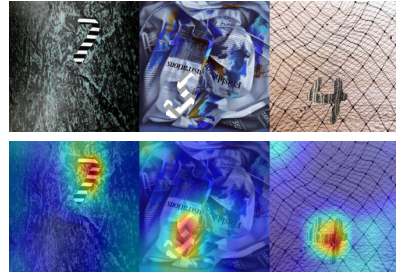


Fig. 7. Grad-CAMs for the model trained with ReFF on Textured MNIST whose digit size is 112. The upper and lower rows show the input images and corresponding Grad-CAMs.

Table 3. Test accuracy [%] vs q on Textured MNIST ($p = 1$ in training dataset). For each condition, we ran the training three times with different random seeds; the standard deviations are shown together. Note that $p = 1$ means that the training dataset does not contain spurious features.

q	Baseline	ReFF
0.0	99.67 ± 0.04	99.70 ± 0.06
0.2	99.60 ± 0.06	99.58 ± 0.04
0.4	99.49 ± 0.06	99.57 ± 0.05
0.6	99.48 ± 0.06	99.53 ± 0.03
0.8	99.53 ± 0.01	99.56 ± 0.06
1.0	99.46 ± 0.05	99.49 ± 0.08

that ReFF does not have any negative effect on training when no spurious features exist.

D. TRAINING DETAILS

Here, we detail the settings of the experiments described in Sec. 4.2.

Classification: The hyperparameter settings are summarized in Tab. 4 (a). We downloaded the initial weights pretrained on ImageNet [5] via `torchvision` library¹. The optimizer settings, except the weight decay, are the default values in PyTorch [6].

Pseudo-annotator: The implementation was done in the same way as `pix2pix` [7]. We set the hyperparameters of the optimizer as shown in Tab. 4 (b). We implemented the discriminator with a 5-layer CNN. The output channels of the layers numbered 64, 128, 256, 512, and 1.

The training procedure of ReFF is shown in Alg. 1

E. REFERENCES

- [1] Noel CF Codella, David Gutman, M Emre Celebi, Brian Helba, Michael A Marchetti, Stephen W Dusza, Aadi Kalloo, Konstantinos Liopyris, Nabin Mishra, Harald

¹<https://pytorch.org/vision/stable/index.html>

Algorithm 1 ReFF training with pseudo-annotator

Input: Regional-annotated training samples $\mathcal{D}_1 = \{(\mathbf{x}_i, y_i, \mathbf{s}_i)\}$,
training samples without regional annotations $\mathcal{D}_2 = \{(\mathbf{x}_i, y_i)\}$

Output: Trained classifier F_θ

Train pseudo-annotator G_ϕ on \mathcal{D}_1

repeat

Sample mini-batch \mathcal{B} from $\mathcal{D}_1 \cup \mathcal{D}_2$

$(\mathcal{L}_{\text{ReFF}}, \mathcal{L}_{\text{main}}) \leftarrow (0, 0)$

for $(\mathbf{x}, y, \mathbf{s})$ in \mathcal{B} **do**

if \mathbf{s} is given **then**

Compute loss l_{ReFF} with Eq. (3)

else

Compute loss l_{ReFF} with Eq. (5)

end if

$\mathcal{L}_{\text{ReFF}} \leftarrow \mathcal{L}_{\text{ReFF}} + l_{\text{ReFF}}$

$\mathcal{L}_{\text{main}} \leftarrow \mathcal{L}_{\text{main}} + l_{\text{main}}$

end for

$\mathcal{L}_{\text{ReFF}} \leftarrow \mathcal{L}_{\text{ReFF}} / |\mathcal{B}|$

$\mathcal{L}_{\text{main}} \leftarrow \mathcal{L}_{\text{main}} / |\mathcal{B}|$

Update θ to minimize $\mathcal{L} = \mathcal{L}_{\text{main}} + \lambda \mathcal{L}_{\text{ReFF}}$

until convergence

▷ Train classifier F_θ

▷ Compute explanation regularizer term

Table 4. Hyperparameter settings of the experiments.

(a) Classification		(b) Pseudo-annotator	
Optimizer	Momentum SGD	Optimizer	Adam
Learning rate	0.01	Learning rate	0.0002
Momentum	0.8	β_1	0.5
Batch size	32	β_2	0.999
Weight decay	10^{-5}	Batch size	4
# of epochs	50	# of iterations	30,000

Kittler, et al., “Skin lesion analysis toward melanoma detection: A challenge at the 2017 international symposium on biomedical imaging (isbi), hosted by the international skin imaging collaboration (isic),” in *International Symposium on Biomedical Imaging (ISBI)*, 2018.

- [2] Omkar M. Parkhi, Andrea Vedaldi, Andrew Zisserman, and C. V. Jawahar, “Cats and dogs,” in *the Conference on Computer Vision and Pattern Recognition*, 2012.
- [3] Masahiro Mitsuhara, Hiroshi Fukui, Yusuke Sakashita, Takanori Ogata, Tsubasa Hirakawa, Takayoshi Yamasita, and Hironobu Fujiyoshi, “Embedding Human Knowledge into Deep Neural Network via Attention Map,” in *International Conference on Computer Vision Theory and Applications*, 2021.
- [4] Hiroshi Fukui, Tsubasa Hirakawa, Takayoshi Yamashita, and Hironobu Fujiyoshi, “Attention Branch Network: Learning of Attention Mechanism for Visual Explanation,” in *the Conference on Computer Vision and Pattern Recognition*, 2019.
- [5] Olga Russakovsky, Jia Deng, Hao Su, Jonathan Krause, Sanjeev Satheesh, Sean Ma, Zhiheng Huang, Andrej

Karpathy, Aditya Khosla, Michael Bernstein, Alexander C. Berg, and Li Fei-Fei, “ImageNet Large Scale Visual Recognition Challenge,” *International Journal of Computer Vision*, vol. 115, no. 3, pp. 211–252, 2015.

- [6] Adam Paszke, Sam Gross, Francisco Massa, Adam Lerer, James Bradbury, Gregory Chanan, Trevor Killeen, Zeming Lin, Natalia Gimelshein, Luca Antiga, Alban Desmaison, Andreas Kopf, Edward Yang, Zachary DeVito, Martin Raison, Alykhan Tejani, Sasank Chilamkurthy, Benoit Steiner, Lu Fang, Junjie Bai, and Soumith Chintala, “PyTorch: An Imperative Style, High-Performance Deep Learning Library,” in *Advances in Neural Information Processing Systems 32*, H. Wallach, H. Larochelle, A. Beygelzimer, F. d’Alché-Buc, E. Fox, and R. Garnett, Eds., pp. 8024–8035. Curran Associates, Inc., 2019.
- [7] Phillip Isola, Jun-Yan Zhu, Tinghui Zhou, and Alexei A. Efros, “Image-To-Image Translation With Conditional Adversarial Networks,” in *the Conference on Computer Vision and Pattern Recognition*, 2017.